Thermal radiation and laminar forced convection in the entrance region of a pipe with axial conduction and radiation

G. Yang and M. A. Ebadian
Department of Mechanical Engineering, Florida International University, Miami, FL, USA

Combined forced convection and thermal radiation in the thermal entrance region of a circular pipe with axial heat conduction and thermal radiation are numerically studied in this article. The fluid is treated as a gray, absorbing and emitting medium with a fully developed velocity entering an isothermal semi-infinite long pipe. The method of moments is applied to approximately model the radiative heat transport process. The governing equations are solved by applying the SIMPLE algorithm. The effects of the Peclet number and its interaction with the conduction–radiation parameter and optical thickness on heat transfer behavior in the thermal entrance region are also investigated. The results obtained indicate that radiation plays a more important role at a low Peclet number than at a high Peclet number and that axial radiation is negligible when the Peclet number $N > 20$. The numerical results for limited cases of no axial heat conduction and radiation are also compared with the available data published in open literature. In all cases, good agreement with these studies was obtained.

Keywords: radiation; axial conduction; combined heat transfer; moments method

Introduction

Axial conduction and axial radiation at low Peclet numbers play an important role in combined heat transfer in a thermally developing pipe flow. In fact, Shah and London[1] and Kakac et al.[2] have extensively reviewed the relevant bibliography about hydrodynamically and thermally developing forced convection flow in a pipe. They have indicated that omitting axial heat conduction introduces an appreciable error in the computation of the heat transfer rate. This can also happen when the fluid involved is a liquid metal, or the flow in the entrance region of the pipes is a low Reynolds number exchanger. Furthermore, the above cited literature indicates that the axial transport effect is negligible only when the Peclet number is greater than 50 in the case of a constant wall temperature and greater than 10 in the case of uniform heat flux along the pipe wall. Investigations by Millsaps and Pohlhausen,[3] Singh,[4] Munakata,[5] Tan and Hsu,[6] Newman,[7] and Michelsen and Villadsen[8] have been directed toward a solution of the heat transfer problem of laminar flow in the entrance region of pipes at a low Peclet number. Millsaps and Pohlhausen,[3] and Singh[4] solved this problem by series expansion, and the first four eigenvalues were calculated. Munakata[5] employed the results of these investigations and showed that fluid axial heat conduction is not negligible for $Pe < 10$. Tan and Hsu,[6] Newman,[7] Michelsen and Villadsen,[8] and Bayazitoglu and Özisik[9] analytically solved the problem of the thermal entrance region subjected to a constant wall temperature. Schmidt and Zeldin,[10] Verhoff and Fisher,[11] and Papoutsakis[12] numerically solved the same problem.

At a high temperature, thermal radiation significantly affects the heat transfer behavior of laminar flow in a pipe. The rigorous formulation of this combined convective–radiative heat transfer problem involves the solution of a nonlinear integro-differential equation. Einstein[13] considered and studied parabolic velocity distributed flow having constant properties with gray fluid in a circular pipe. Pearce and Emery[14] solved the same problem with both uniform and parabolic velocity distributions using the box method technique. Echigo et al.[15] analyzed gas flow as a conjugated problem in the fluid domain. Using finite-difference techniques, these authors examined the energy equation with two-dimensional radiative heat transfer allowing an upstream propagation from the entrance of the heating section. Yener and Fong[16] investigated simultaneous radiation and forced convection in a thermally developing laminar flow. They solved the radiative equation with isotropic scattering using the Fourier series technique.

Campo and Schuler[17] modeled the radiation transport process applying the method of moments (cf. Özisik[18]) and numerically solved the combined heat transfer problem. The method of moments is an approximation method using a system of partial differential equations to replace the integro-differential equation. Furthermore, their predicted results are in excellent agreement with Pearce and Emery[14] and Echigo et al.[15] Therefore, it is evident from the literature cited that most of these investigators are omitting either axial heat conduction, axial radiation, or both in their energy equations. However, neglecting axial heat conduction and axial radiation in the entrance region of a pipe at a low Peclet number causes a significant error in heat transfer results. Recently, Kim and Lee[19] studied combined heat transfer in a thermally developing Poiseuille flow considering anisotropic scattering radiation. By employing the S-N discrete ordinant method to model the radiation effect, they reported the temperature profile and bulk temperature distribution. However, no Nusselt number distribution has been given in their paper.

The above literature survey indicates that the effects of axial conduction and axial radiation have not been extensively investigated for the case of combined forced convection and thermal radiative heat transfer in a circular pipe. Therefore, the

Address reprint requests to Dr. Yang at the Department of Mechanical Engineering, Florida International University, Miami, FL 33199, USA.

Received 18 October 1990; accepted 4 April 1991

objective of this paper is to present a numerical solution considering the combined effects of axial heat conduction and thermal radiation. Special attention has been devoted to what effect a small Peclet number has on the characteristics of this combined heat transfer process.

Problem formulation

Basic assumptions and governing equations

Shah and London[1] have summarized three sets of initial and boundary conditions for the extended Graetz problem. Figure 1 illustrates the type A conditions as documented in their book. Since it does not take into account the effects of preheating before the fluid enters the pipe, the type A boundary condition may result in considerable error for many cases. However, type A initial and boundary conditions may be a valid idealization if good fluid mixing is obtained in the inlet header of a heat exchanger.[1] The participating gas flows into a circular pipe with a parabolic velocity profile and a uniform entrance temperature, T_e, at starting point, $x=0$. The surface temperature of the pipe is maintained at T_w ($T_w > T_e$). The coordinate system and the physical model are also illustrated in Figure 1. With the following assumptions that (1) the working medium is an incompressible steady hydraulic fully developed laminar flow with constant physical properties; and (2) the gas is assumed to be a gray, emitting, absorbing, and nonscattering medium, the governing equations describing convective–radiative heat transfer inside a circular pipe can be written as follows:

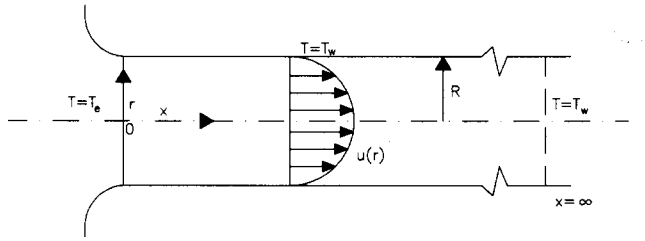

Figure 1 Geometry and coordinate system

$$\rho C_p u \frac{\partial T}{\partial x} = k\left[\frac{\partial^2 T}{\partial x^2} + \frac{1}{r}\frac{\partial}{\partial r}\left(r\frac{\partial T}{\partial r}\right)\right] - \operatorname{div} \vec{q} \tag{1}$$

In energy Equation 1, the last term on the right-hand side represents the contribution of gas radiation that can be modeled by the method of moments (cf. Özisik[18]). Previous studies indicate that approximation of the moment is more accurate in the optically thick rather than the optically thin limit. However, for the realistic case of nongray gaseous radiation, a major portion of the emission and absorption of thermal radiation occurs near the band center, where the medium is optically thick at these frequencies. Therefore, the inaccuracy of the method of moments at the optically thin region is not a limitation of its application to the nongray medium.

$$\operatorname{div} \vec{q} = -\int_{4\pi} \kappa[I_0(\vec{\Omega}, S) - I_b(T)]\, d\omega = -\kappa(G - 4\sigma T^4) \tag{2}$$

where irradiation, $G = 4\pi I_0$, can be found by solving

$$\frac{\partial^2 G}{\partial x^2} + \frac{1}{r}\frac{\partial}{\partial r}\left(r\frac{\partial G}{\partial r}\right) = 3\beta\kappa(G - 4\sigma T^4) \tag{3}$$

The fully developed gas velocity, u, will be in the form of:

$$u(r) = 2u_m(1 - r^2/R^2) \tag{4}$$

The boundary conditions for Equations 1 and 3 are

$$@\ x=0 \qquad T = T_e = \text{constant} \qquad 0 < r < R \tag{5a}$$

$$\frac{\partial G}{\partial X} = -\tfrac{3}{2}\kappa(G - 4\sigma T_e^4) \qquad 0 < r < R \tag{5b}$$

$$@\ x>0 \qquad T|_{r=R} = T_w \tag{5c}$$

Notation

A Variable coefficient, Equation 13
B Variable coefficient, Equation 14
C_p Specific heat [J kg^{-1} K^{-1}]
D_h Hydraulic diameter of the pipe $=2R$ [m]
G Total irradiation [W m^{-2}]
G^* Dimensionless value of G, Equation 6
I Intensity of radiation [W m^{-2} sr^{-1}], Equation 2
k Thermal conductivity [W m^{-1} K^{-1}]
N Conduction–radiation parameter, Equation 6
Pe Peclet number, Equation 6
Pr Prandtl number, $\Pr = \nu/\alpha$
q Heat flux [W m^{-2}], Equation 1
r Dimensional radial coordinate [m]
R Radius of the pipe [m]
Re Reynolds number, $\mathrm{Re} = (u_m D_h)/\nu$
S Path vector, Equation 2
T Temperature of fluid [K]
u Velocity [m s^{-1}]
u_m Mean velocity [m s^{-1}]
u^* Dimensionless velocity
$u^\#$ Artificial velocity in the η direction, Equation 17
$v^\#$ Artificial velocity in the ξ direction, Equation 17
x Dimensionless axial coordinate [m]
x^* Dimensionless axial coordinate

Greek symbols
α Thermal diffusivity [m^2 s^{-1}]
β Extinction coefficient [m^{-1}]
$\Gamma^\#_{\phi\eta}$ Artificial viscosity in the η direction, Equation 17
$\Gamma^\#_{\phi\xi}$ Artificial viscosity in the ξ direction, Equation 17
ε_w Emissivity of wall
η Dimensionless axial coordinate
θ Dimensionless temperature, T/T_w
θ_b Dimensionless bulk temperature, T_b/T_w
θ_e Dimensionless inlet temperature, T_e/T_w
κ Volumetric absorption coefficient [m^{-1}]
μ Dynamic viscosity [kg m^{-1} s^{-1}]
ν Kinematic viscosity [m^2 s^{-1}]
ξ Dimensionless radial coordinate
ρ Density [kg m^{-3}]
σ Stefan–Boltzmann constant [W m^{-2} K^{-4}]
τ Optical thickness
ϕ General dimensionless variable, Equation 17
Ω Direction, Equation 2

Subscripts
b Mean bulk
c Conduction
e Entrance
r Radiation
t Total
w Wall (circumferential)

$$\partial G/\partial r|_{r=R} = -\frac{3\varepsilon_w \kappa}{2(2-\varepsilon_w)}(G-4\sigma T_w^4) \quad (5d)$$

$$\partial T/\partial r|_{r=0} = 0 \quad (5e)$$

$$\partial G/\partial r|_{r=0} = 0 \quad (5f)$$

$$@\ x=\infty \quad T=T_w \quad 0<r<R \quad (5g)$$

$$\frac{\partial G}{\partial X} = 0 \quad 0<r<R \quad (5h)$$

Since the opening of the inlet duct is nonreflecting, the assumption of a pseudo black wall is applied for the radiation boundary condition in Equation 5b. At the outlet of the duct, the uniform temperature distribution suggests that incident radiation, G, will not change with the axial location, as given in Equation 5h.

Dimensionless governing equation

By introducing the following dimensionless quantities,

$$x^* = x/(D_h \mathrm{Pe}) \quad \xi = r/R \quad \theta = T/T_w \quad u^* = u/u_m$$
$$G^* = G/(4\sigma T_w^4) \quad D_h = 2R \quad N = (k\kappa)/(4\sigma T_w^3) \quad (6)$$
$$\tau = \kappa D_h \quad \mathrm{Pe} = \mathrm{RePr} = (u_m D_h)/\alpha$$

governing Equations 1 and 3 can be written as:

$$u^* \frac{\partial \theta}{\partial x^*} = \frac{1}{\mathrm{Pe}^2}\frac{\partial^2 \theta}{\partial x^{*2}} + \frac{4}{\xi}\frac{\partial}{\partial \xi}\left(\xi \frac{\partial \theta}{\partial \xi}\right) + \frac{\tau^2}{N}(G^* - \theta^4) \quad (7)$$

and

$$\frac{1}{\mathrm{Pe}^2}\frac{\partial^2 G^*}{\partial x^{*2}} + \frac{4}{\xi}\frac{\partial}{\partial \xi}\left(\xi \frac{\partial G^*}{\partial \xi}\right) = 3\tau^2(G^* - \theta^4) \quad (8)$$

Transformation of the governing equations

Due to the fact that the boundary condition at $x=\infty$ is difficult to manage in the numerical process, a coordinate transformation is conducted. By introducing a new coordinate variable, η, as suggested by Verhoff and Fisher[11],

$$x^* = \tan\left(\frac{\pi}{2}\eta\right), \quad (9)$$

governing Equations 7 and 8 become

$$\left(u^*(\xi)A(\eta) + \frac{B(\eta)}{\mathrm{Pe}^2}\right)\frac{\partial \theta}{\partial \eta} = \frac{A(\eta)^2}{\mathrm{Pe}^2}\frac{\partial^2 \theta}{\partial \eta^2} + \frac{4}{\xi}\frac{\partial}{\partial \xi}\left(\xi \frac{\partial \theta}{\partial \xi}\right) + \frac{\tau^2}{N}(G^* - \theta^4) \quad (10)$$

$$\frac{B(\eta)}{\mathrm{Pe}^2}\frac{\partial G^*}{\partial \eta} = \frac{A(\eta)^2}{\mathrm{Pe}^2}\frac{\partial^2 G^*}{\partial \eta^2} + \frac{4}{\xi}\frac{\partial}{\partial \xi}\left(\xi \frac{\partial G^*}{\partial \xi}\right) - 3\tau^2(G^* - \theta^4) \quad (11)$$

Accordingly, the boundary conditions will also transform to

$$@\ \eta=0 \quad \theta = \theta_e = \text{constant} \quad \theta<\xi<1 \quad (12a)$$

$$\partial G^*/\partial \eta = -\frac{3\tau}{2A(\eta)}(G^* - \theta_e^4) \quad 0<\xi<1 \quad (12b)$$

$$@\ 1>\eta>0 \quad \theta|_{\xi=1} = 1 \quad (12c)$$

$$\partial G^*/\partial \xi|_{\xi=1} = -\frac{3\varepsilon_w}{2(2-\varepsilon_w)}\tau(G^* - 1) \quad (12d)$$

$$\partial \theta/\partial \xi|_{\xi=0} = 0 \quad (12e)$$

$$\partial G^*/\partial \xi|_{\xi=0} = 0 \quad (12f)$$

and

$$@\ \eta=1 \quad \theta = 1 \quad 0<\xi<1 \quad (12g)$$

$$\frac{\partial G^*}{\partial \eta} = 0 \quad 0<\xi<1 \quad (12h)$$

where

$$A(\eta) = \frac{2}{\pi}\cos^2\left(\frac{\pi}{2}\eta\right) \quad (13)$$

$$B(\eta) = \frac{4}{\pi}\cos^3\left(\frac{\pi}{2}\eta\right)\sin\left(\frac{\pi}{2}\eta\right). \quad (14)$$

The mean bulk temperature and Nusselt number

The physical quantities of interest in heat transfer study are the mean bulk temperature and the Nusselt number. The mean bulk temperature is defined by

$$\theta_b(\eta) = \frac{\int_0^1 \theta(\eta, \xi)u^*(\xi)\xi\, d\xi}{\int_0^1 u^*(\xi)\xi\, d\xi} \quad (15)$$

and the Nusselt number is

$$\mathrm{Nu}_t = \mathrm{Nu}_c + \mathrm{Nu}_r = \frac{2}{\theta_b}\frac{d\theta}{d\xi}\bigg|_{\xi=1} - \frac{1}{2\theta_b}\frac{\tau}{N}\left(\frac{\varepsilon_w}{2-\varepsilon_w}\right)(G_w^* - 1) \quad (16)$$

The subscripts, t, c, and r, represent total, convective, and radiative heat transfer, respectively.

Numerical analysis

Equations 10 and 11 are nonlinear parabolic partial differential equations. If artificial velocities, $u^\#$ and $v^\#$, and nonisotropic viscosities, $\Gamma^\#_{\phi\eta}$ and $\Gamma^\#_{\phi\xi}$, are introduced, both equations can be written in standard form as[20]

$$\frac{\partial}{\partial \eta}(u^\# \phi) + \frac{1}{\xi}\frac{\partial}{\partial \xi}(\xi v^\# \phi) = \frac{\partial}{\partial \eta}\left(\Gamma^*_{\phi\eta}\frac{\partial \phi}{\partial \eta}\right) + \frac{1}{\xi}\frac{\partial}{\partial \xi}\left(\xi\Gamma^*_{\phi\xi}\frac{\partial \phi}{\partial \xi}\right) + S_u + S_p \quad (17)$$

where the quantities for each term in the above equation are documented in Table 1.

The SIMPLE algorithm of Patankar[20] was applied for solving the above equations subjected to the associated boundary conditions. Equal space grids are used in both radial and axial directions. It should be noted that the axial coordinate has been transformed by a tangential function, which means having a small step size near the entrance region that grows larger downstream in the physical domain. The two equations are solved sequentially, and the iteration process is terminated when maximum variation of any nodal value (θ and G^*) is less than 10^{-5} in two successive iterations. To ensure the accuracy of the numerical solution, an independent grid size test has been conducted in this study. Table 2 depicts the results of this test with differential mesh sizes. The conductive–radiative parameter, optical thickness, and the Peclet number used in this test case are $N=0.2$, $\tau=2$, and $\mathrm{Pe}=5$, respectively. These data indicate that almost identical results can be obtained when the grid size is more than 40×20 (axial by radial). Therefore, the grid size 40×20 is mainly used throughout this study for computation of the Nusselt number. The number of iterations to achieve a convergence solution strongly depends on the Peclet number and not on the other parameters. The smaller the Peclet number, the more iterations are required. Approximately 250 iterations are needed for a Peclet number equal to 1, while approximately 100 iterations are needed for

Table 1 Variables defined in Equation 17

Equation, ϕ	u^*	v^*	$\Gamma^*_{\phi\eta}$	$\Gamma^*_{\phi\xi}$	S_u	S_p
Energy equation, θ	$\frac{1}{4}\left(uA+\frac{B}{Pe^2}\right)$	0	$\frac{1}{4}\frac{A^2}{Pe^2}$	1	$\frac{1}{4}\frac{\tau^2}{N}G^*$	$-\frac{1}{4}\frac{\tau^2}{N}\theta^3$
Irradiation equation, G^*	$\frac{1}{4}\frac{B}{Pe^2}$	0	$\frac{1}{4}\frac{A^2}{Pe^2}$	1	$\frac{3}{4}\tau^2\theta^4$	$-\frac{3}{4}\tau^2$

Table 2 The effect of grid size on the local Nusselt number

	$M\times N$		
	30 × 15	40 × 20	80 × 40
X^*		Nu	
0.0056	23.4	25.6	25.8
0.0170	12.1	12.0	11.7
0.0512	8.26	8.24	8.22
0.1030	10.4	10.4	10.4
0.1510	13.1	13.2	13.2
0.2660	16.8	18.0	17.8
0.3870	17.4	21.9	21.4

a Peclet number greater than 100. For the case of a large τ and small N, more grids have been employed due to the convergence problem. The number of grids used is more sensitive to τ, since the source term is proportional to τ^2/N. The 120 × 80 grid can give a convergence solution for the case of $\tau^2/N<400$. Relaxation coefficients have been used to further increase τ^2/N. For example, with the relaxation coefficients equal to 0.7 for both equations, the convergence solution can attain a value of $\tau^2/N<80{,}000$. However, CPU time will be tripled to satisfy the convergence criteria.

Assessment of the validity of the proposed methodology

In order to assess the validity of the proposed methodology and the associated computer program, several limiting case solutions are documented in this paper. As mentioned earlier, no analytical and/or experimental data are available for the case of combined modes of heat transfer, including the effects of axial conduction and radiation with the boundary conditions of Equation 12. Therefore, the only available means for verification is through comparison with the limiting case solutions available from previous investigations.

By setting $N=\infty$, the problem reduces to a case of pure convection. Figure 2 shows a comparison of the Nusselt number variations in the entrance region with Schmidt and Zeldin.[10] The predicted values in this study are in excellent agreement with those given by Schmidt and Zeldin.[10]

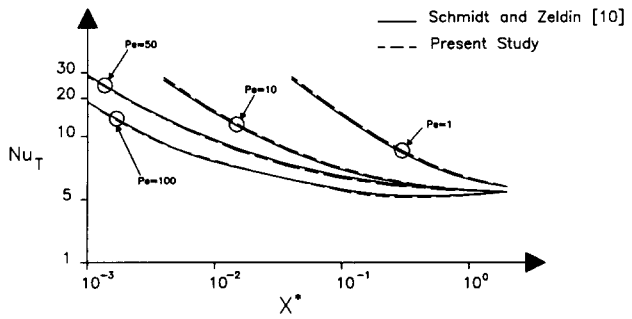

Figure 2 Local Nusselt number variation for the case of no radiation

Comparisons of the limited case for the combined heat transfer model with large Peclet numbers are given in Figures 3 and 4. Figure 3 shows a comparison of the predicted results between Echigo et al.[15] and the present study. The results of Echigo et al.[15] are obtained from an integro-differential equation at Pe = 1,000, in which axial conduction and axial radiation in this region can be safely disregarded. This figure indicates some deviation in the immediate entrance region for both Nu_c and Nu_t. The deviations between the two predictions reduce rapidly as x^* increases. A comparison is also conducted with the results of Pearce and Emery[14] for a larger region in the axial direction, as shown in Figure 4. This figure further illustrates that the present radiative model can accurately predict the combined heat transfer behavior.

Numerical results and discussion

The problem of combined thermal radiation and forced convection heat transfer with axial heat conduction and axial radiation contains many physical parameters. The governing

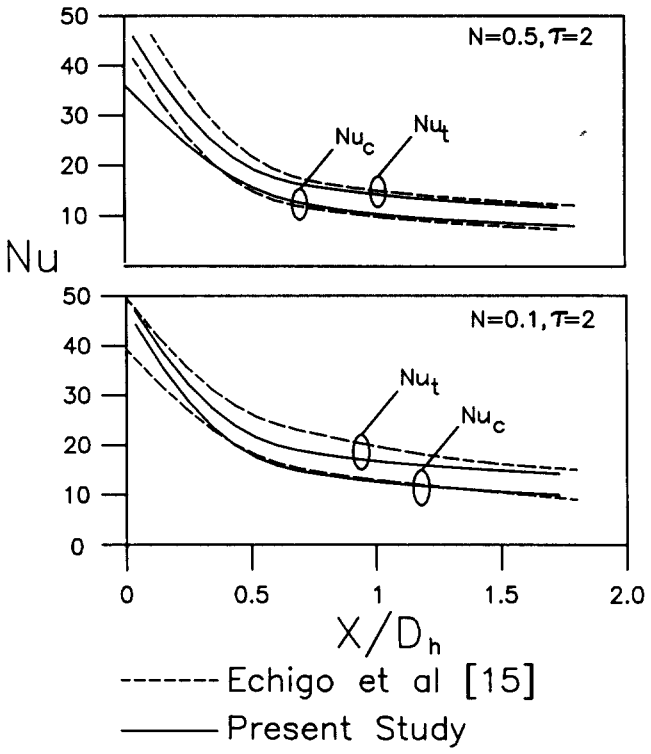

Figure 3 Local Nusselt number variation for the case of no axial heat conduction and radiation

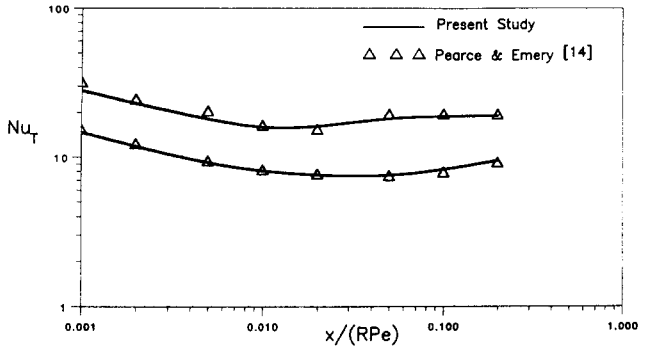

Figure 4 Total Nusselt number variation for the case of axial radiation only

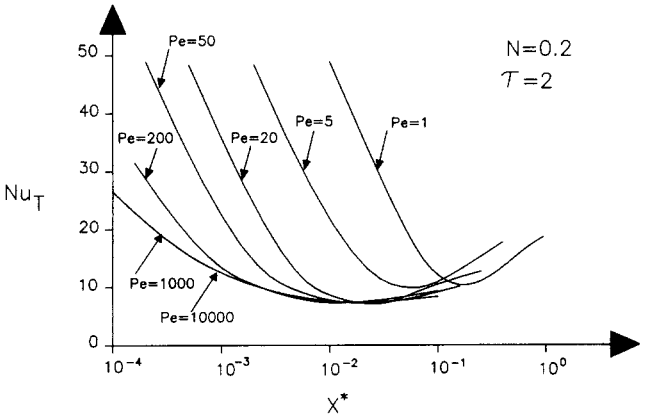

Figure 5 Effects of the Peclet number on the total Nusselt number

equations and the associated boundary conditions indicate that the parameters controlling the problem are (1) the Peclet number, Pe; (2) the conductive–radiative parameter, N; and (3) optical thickness, τ. The numerical solutions are generated for various combinations of these parameters, and the effects of N and τ on combined heat transfer in a circular pipe are extensively studied. This paper focuses on the effects of the Peclet number, as well as its interactions with N and τ.

The effects of the Peclet number on the local Nusselt number for flow inside the pipes are shown in Figure 5. The Peclet number represents the relative magnitude of thermal energy convected to the fluid and thermal energy axially conducted within the fluid. In this figure, the conduction–radiation parameter, N, and optical thickness, τ, are equal to 0.2 and 2, respectively. Seven different Peclet numbers ranging from 1 to 1,000 have been used. Basically, these curves exhibit the same behavior as the nonradiative case, where a decrease in the Pe number results in an increase of the local Nusselt number. However, when the Peclet number reaches 1,000, $Nu-x/(D_h\mathrm{Pe})$ no longer depends on the Peclet number. It should be noted that unlike the nonradiative case, the curves in this figure demonstrate that a state of full thermal development is never reached (cf. Pearce and Emery,[14] Lii and Özisik,[21] Yener and Fong,[16] and Campo and Schuler[17]). For instance, in the case of Pe=1, the total Nusselt number curve attains a minimum value at a certain downstream location and beyond that point, Nu_t increases again. This phenomenon can be explained by the fact that the Nusselt number contributed by convection decreases along the pipe, while the Nu contributed by radiation increases. Forced convection is dominant at the entrance region of the pipe. However, as the fluid passes through the pipe, radiation influences heat transfer behavior. This same tendency has also been observed by Pearce and Emery[14] and Yener and Fong.[16]

Figure 6 illustrates the effects of the Peclet number on the transverse temperature profile at $x=2D_h$. During calculations, $N=0.2$ and $\tau=2$ are used. At very high values of Pe (1,000 and 10,000), the convection is very strong and the inlet temperature is carried into the pipe in the core region for a considerable distance. In these two cases, the thermal boundary layer does not yet unify. However, unlike pure convection, the uniform temperature in the core region is slightly higher than the inlet temperature, θ_e. This is due to energy absorption by radiation. As the Pe number decreases, a thermal boundary layer merger occurs at the centerline and the parabolic temperature profile appears. For low Pe numbers of 1 and 5, thermal radiation dominates the energy transport, and thermal uniformity is nearly reached.

The effects of axial conduction and axial radiation on heat transfer in the thermal entrance region of a circular pipe are shown in Tables 3 through 5. Three cases are discussed in these tables: Case 1, with both axial conduction and axial radiation; Case 2, with axial conduction, but neglecting axial radiation (one-dimensional radiation model); and Case 3, which neglects both axial conduction and radiation. Table 3 illustrates the interaction between the Peclet number and conduction–radiation parameter, N, in the thermal entrance region with optical thickness, $\tau=3$. It is worth noting that neglecting axial energy transfer will overestimate the heat transfer rate in the immediate entrance region and underestimate it downstream. The overestimate region for Case 3 is usually much shorter than that for Case 2. Furthermore, the Nu number deviation of Case 3 from Case 1 is much higher than that of Case 2 for both the overestimate and underestimate regions. This phenomena is mainly due to the axial temperature gradient forcing the energy transfer in a downstream direction. It is also worthy to note that for the case of weak radiation, axial conduction plays an important role on heat transfer, and axial radiation is not so significant. For example, at the Pe=5 and $N=1$ conditions, neglecting axial conduction can result in a 55 percent overestimation of the Nusselt number in the immediate entrance region, while the Nusselt number deviation is only 3 percent when neglecting axial radiation. However, in a condition of strong radiation, neglecting axial radiation can result in a significant error in the entrance region, as observed in Cases 2

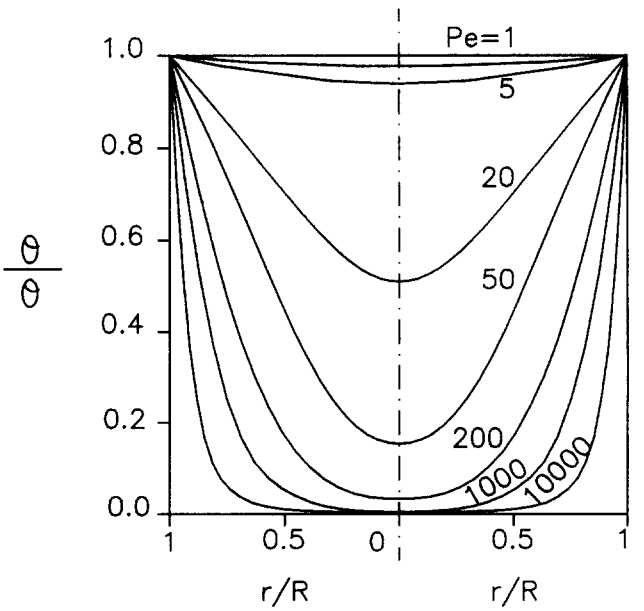

Figure 6 Effects of the Peclet number on the temperature profile

Table 3 Total Nusselt number affected by the interaction of Peclet number and conduction–radiation parameter

	Pe=5 τ=3.0								
	N=1.0			N=0.25			N=0.1		
x	1*	2†	3‡	1*	2†	3‡	1*	2†	3‡
0.001	7.03	7.24	10.90	8.87	9.95	12.70	12.6	16.6	16.7
0.004	6.68	6.87	7.44	8.64	9.65	9.31	13.6	16.6	13.4
0.012	6.02	6.18	5.48	8.43	9.20	7.58	14.6	17.1	12.8
0.020	5.67	5.79	4.97	8.55	9.09	7.41	16.9	18.0	14.3
0.041	5.32	5.36	4.73	9.60	9.50	8.44	23.5	21.3	21.6
0.070	5.34	5.31	4.96	11.40	10.60	10.70	29.1	25.6	29.4
0.102	5.59	5.44	5.32	12.90	11.80	12.90	31.6	28.7	32.7
0.131	5.85	5.61	5.59	13.90	12.80	14.30	32.5	30.3	33.1
0.150	6.03	5.72	5.73	14.30	13.30	14.80	32.9	31.0	33.2
	Pe=20 τ=3.0								
	N=1.0			N=0.25			N=0.1		
x	1*	2†	3‡	1*	2†	3‡	1*	2†	3‡
0.001	10.10	10.20	11.20	11.70	12.00	13.00	14.7	16.0	16.7
0.002	8.61	8.66	8.42	10.30	10.50	10.20	13.5	14.6	14.0
0.005	7.08	7.11	6.68	8.87	9.05	8.50	12.7	13.4	12.5
0.007	6.46	6.48	6.09	8.34	8.46	7.96	12.6	13.1	12.2
0.011	5.73	5.74	5.53	7.87	7.85	7.51	13.0	13.1	12.3
0.015	5.34	5.33	5.11	7.62	7.60	7.28	13.9	13.6	12.9
0.021	5.06	5.05	4.87	7.60	7.54	7.29	15.3	14.6	14.1
0.041	4.77	4.76	4.67	8.50	8.33	8.23	22.8	20.7	20.7
0.070	4.95	4.92	4.90	10.80	10.30	10.30	29.9	28.1	28.7
0.100	5.25	5.20	5.19	12.90	12.40	12.50	32.0	31.7	32.8
	Pe=200 τ=3.0								
	N=1.0			N=0.25			N=0.1		
x	1*	2†	3‡	1*	2†	3‡	1*	2†	3‡
0.0001	23.80	23.80	23.80	25.60	25.70	25.70	29.2	29.5	29.5
0.0003	16.50	16.50	16.10	18.30	18.40	18.00	21.9	22.0	21.7
0.0005	13.80	13.80	13.50	15.60	15.60	15.40	19.2	19.3	19.0
0.0010	14.00	14.00	13.90	12.70	12.80	12.60	16.3	16.4	16.3
0.0020	8.71	8.70	8.66	10.50	10.50	10.40	14.1	14.1	14.1
0.0040	7.06	7.06	7.04	8.85	8.84	8.82	12.7	12.7	12.6
0.0070	6.04	6.04	6.03	7.89	7.89	7.88	12.1	12.0	12.0
0.0100	5.53	5.53	5.52	7.47	7.47	7.46	12.1	12.0	12.0
0.0300	4.58	4.68	4.68	7.48	7.48	7.48	16.2	16.1	16.1
0.0500	4.69	4.69	4.69	8.67	8.67	8.67	21.5	21.5	21.5

* With axial conduction and axial radiation.
† With axial conduction without axial radiation.
‡ Without axial conduction and axial radiation.

Table 4 Contribution of convection and radiation on total Nusselt number (Pe=5, τ=3.0, N=0.1)

	Case 1			Case 2			Case 3		
	Nu_c	Nu_r	Nu_t	Nu_c	Nu_r	Nu_t	Nu_c	Nu_r	Nu_t
0.001	6.49	6.14	12.64	7.07	9.50	16.6	9.65	7.05	16.7
0.004	6.20	7.75	12.95	6.76	9.80	16.6	6.21	7.23	13.4
0.012	5.90	8.73	14.60	6.32	10.70	17.1	4.62	8.21	12.8
0.020	5.88	11.10	16.90	6.10	11.90	18.0	4.56	9.70	14.3
0.041	5.80	17.70	23.50	5.95	15.30	21.3	4.44	17.20	21.6
0.070	5.71	23.30	29.10	5.81	19.80	25.6	4.27	25.10	29.4

and 3 for Pe=5 and N=0.1 conditions. Derived from the assumption of the boundary layer flow, Sparrow and Cess[22] have proposed a criterion, $N\text{Pe} \gg 1$, to determine when axial radiation is negligible. From Table 3, it is evident that axial radiation can safely be neglected when $\text{Pe}N > 20$, as shown in the Case 2 for the conditions of Pe=20, N=1, or Pe=200, N=0.1. However, axial conduction cannot be neglected in Case 3 for conditions of Pe=20 and N=1, since Pe<50, as mentioned in Figure 5.

The data in Table 3 illustrate the same tendency as in the

Table 5 Nu_T affected by the interaction between Peclet number and optical thickness

Pe = 5, N = 0.25												
	τ = 1			τ = 3			τ = 10			τ = 20		
x	1	2	3	1	2	3	1	2	3	1	2	3
0.001	6.94	7.20	10.90	8.87	9.95	12.70	13.3	15.8	16.8	15.7	18.3	19.2
0.004	6.58	6.83	7.42	8.64	9.65	9.31	13.8	15.3	12.8	16.3	17.4	14.1
0.012	5.91	6.15	5.48	8.43	9.20	7.58	15.5	14.7	10.9	17.6	16.1	11.8
0.020	5.54	5.78	4.98	8.55	9.09	7.41	16.8	14.7	11.2	18.3	15.9	12.2
0.049	5.15	5.37	4.74	9.60	9.50	8.44	18.9	16.2	15.0	19.7	17.4	17.0
0.070	5.22	5.35	5.02	11.40	10.60	10.70	20.5	18.8	19.4	21.0	20.3	22.0
0.102	5.57	5.57	5.52	12.90	11.80	12.90	21.5	20.8	21.0	22.1	22.4	24.5
0.131	6.02	5.83	6.00	13.90	12.80	14.30	22.2	21.8	22.3	22.8	23.3	24.9
0.150	6.39	6.03	6.31	14.30	13.30	14.80	22.4	22.4	23.6	23.1	23.7	24.9
Pe = 20, N = 0.25												
	τ = 1			τ = 3			τ = 10			τ = 20		
x	1	2	3	1	2	3	1	2	3	1	2	3
0.001	10.10	10.20	11.20	11.70	12.00	13.00	14.7	16.3	16.9	16.6	18.9	19.3
0.002	8.56	8.64	8.40	10.30	10.50	10.20	13.6	14.4	13.7	15.6	16.3	15.2
0.005	7.04	7.10	6.67	8.87	9.05	8.50	12.5	12.5	11.6	14.1	13.8	12.7
0.007	6.41	6.47	6.08	8.34	8.46	7.96	12.1	11.8	11.0	13.5	12.9	11.9
0.011	5.70	5.74	5.45	7.87	7.85	7.51	11.6	11.2	10.5	12.8	12.1	11.4
0.015	5.30	5.33	5.11	7.62	7.60	7.28	11.6	11.0	10.5	12.7	12.0	11.4
0.021	5.04	5.05	4.88	7.60	7.54	7.29	11.9	11.3	10.9	13.1	12.4	11.9
0.041	4.78	4.76	4.68	8.50	8.33	8.23	15.4	14.7	14.7	17.4	16.6	16.7
0.070	4.99	4.93	4.90	10.80	10.30	10.30	19.7	19.1	19.1	21.9	22.2	22.3
0.100	5.36	5.22	5.21	12.90	12.40	12.50	21.3	20.9	20.5	23.8	24.2	24.7
Pe = 200, N = 0.25												
	τ = 1			τ = 3			τ = 10			τ = 20		
x	1	2	3	1	2	3	1	2	3	1	2	3
0.0001	23.80	23.80	23.70	25.60	25.70	25.70	30.4	30.7	30.8	34.4	35.5	35.5
0.0003	16.50	16.50	16.10	18.30	18.40	18.00	22.9	23.0	22.5	26.4	26.5	25.9
0.0005	13.80	13.80	13.50	15.60	15.60	15.40	19.9	19.9	19.6	22.9	22.8	22.5
0.0010	10.90	11.00	10.80	12.70	12.80	12.60	16.7	16.6	16.5	18.9	18.8	18.7
0.0020	8.68	8.70	8.64	10.50	10.50	10.40	14.0	13.9	13.9	15.5	15.5	15.4
0.0040	7.05	7.07	7.03	8.85	8.84	8.82	12.0	12.0	11.9	13.1	13.1	13.1
0.0070	6.04	6.05	6.02	7.89	7.89	7.88	10.9	10.9	10.9	11.8	11.8	11.7
0.0100	5.52	5.52	5.51	7.47	7.47	7.46	10.5	10.5	10.4	11.3	11.3	11.3
0.0300	4.66	4.70	4.66	7.48	7.48	7.48	12.2	12.2	12.2	13.5	13.5	13.5
0.0500	4.66	4.72	4.66	8.67	8.67	8.67	16.2	16.2	16.2	18.5	18.5	18.5

discussion for Figure 5; i.e., the total Nu decreases at the inlet and reaches a minimum value, then increases again. However, when Pe = 5 and N = 0.1, a different trend is shown. In this case, the Nu continuously increases along the axial direction. The reason for this tendency can be explained by Table 4. Table 4 breaks down the total Nusselt number into two parts: the heat transfer contributed by convection, Nu_c, and the heat transfer contributed by radiation, Nu_r. The convection contribution shows the same trend as in the condition of pure convection heat transfer in which the Nusselt number decreases as x increases. However, the radiation contribution increases much faster than the decrease of the convection contribution, which results in a continuous increase for the total Nusselt number. These phenomena occur only in the case of a small Peclet number with strong thermal radiation.

Figure 7 illustrates the interaction of gas optical thickness and the Peclet number effect on the thermal heat transfer behavior in the entrance region. Parameter τ is the measure of the capability of the medium to absorb radiation. In Figure 7a, conduction–radiation parameter, N, and the Peclet number are equal to 0.25 and 200, respectively, in which the axial energy transportation can be neglected. This figure indicates that initially the total Nusselt number increases as τ increases. However, for a very large optical thickness, Nu decreases as τ increases, since the medium becomes too thick for electromagnetic waves to penetrate. Therefore, the case of $\tau = \infty$ is the same as that of $\tau = 0$. At Pe = 5, the case with a strong axial energy transport, the $Nu - \tau$ relation exhibits a different behavior from Pe = 200, as seen in Figure 7b. At small τ ($\tau = 1$), the Nusselt number decreases and then rises, which is similar to that found in Pe = 200. When $\tau = 3$, the Nu rises sharply after passing the saddle point. When $\tau = 10$ and 20, the Nu continuously rises from the beginning and no saddle point exists. Table 5 shows the effects of the interaction of the Peclet number and the optical thickness on heat transfer behavior. The same three cases discussed in Table 3 are used. One thing worth

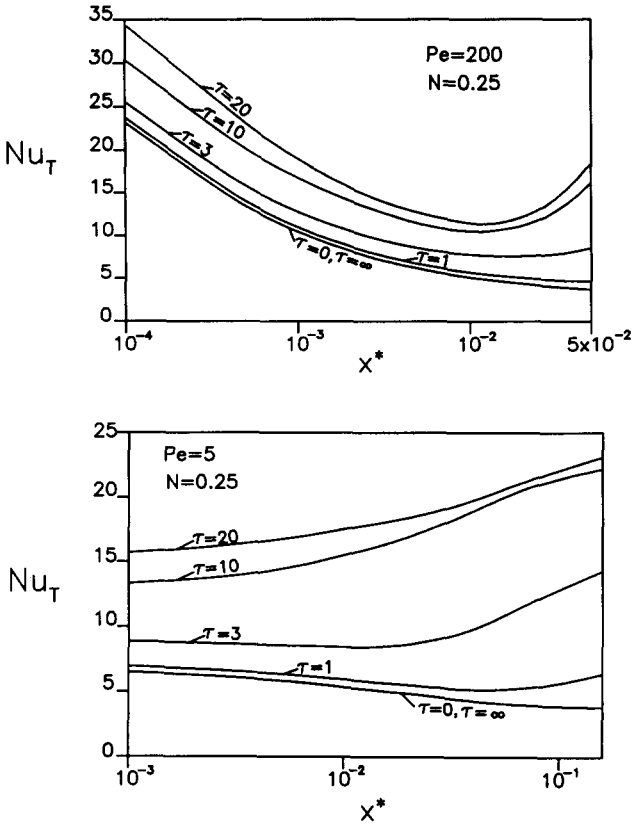

Figure 7 Effects of the interaction of Pe and τ on the total Nusselt number

noting when axial radiation is neglected, the Nu variation increases as τ increases. For example, in the case of $Pe=20$, $N=0.25$, the deviations at the inlet are 1, 2.6, 11, and 14 percent for the cases of $\tau=1$, 3, 10, and 20, respectively. However, axial energy transfer can safely be neglected when $PeN>50$ at all values of τ, since deviations can be controlled at 3 percent.

Conclusion

Combined thermal radiation and laminar forced convection with axial conduction and axial radiation in a circular pipe have been investigated. Thermal radiation is modeled by the method of moments. The governing equations are transformed by an inverse tangent transformation to convert the infinite boundaries to finite boundaries. The working governing equations are solved by applying the SIMPLE algorithm. The effects of the Peclet number, conduction–radiation parameter, and optical thickness on heat transfer behavior in the thermal entrance region of a circular pipe have been investigated. The study shows that the Peclet number is the first important parameter when considering the effects of axial conduction and axial radiation. Furthermore, the contributions of optical thickness, τ, and the conduction–radiation parameter, N, on heat transfer will be enhanced as the Peclet number decreases. The results also show that the criterion to neglect axial radiation may also be related to the optical thickness, τ, especially at the small Peclet number. However, axial thermal radiation can be safely neglected when $PeN>50$.

Acknowledgment

The results presented in this paper were obtained in the course of research sponsored by the Department of Energy under Subcontract No. 19X-SE133V.

References

1 Shah, R. K., and London, A. L. *Laminar Flow Forced Convection in Ducts.* Academic Press, New York, 1978
2 Kakac, S., Shah, R. K., and Aung, W. *Handbook of Single-Phase Convective Heat Transfer.* Wiley Interscience, New York, 1987, 4–83
3 Millsaps, K., and Pohlhausen, K. Heat transfer to hagen-poiseuille flows. *Proc. Conference on Differential Equations* (J. B. Diaz and L. E. Payne, eds.), University of Maryland Bookstore, College Park, 1956, 271–294
4 Singh, S. N. Heat transfer by laminar flow in a cylindrical tube. *Appl. Sci. Res. Sect. A*, 1958, **7**, 325–340
5 Munakata, T. The calculation of laminar heat transfer in a tube. *Int. Chem. Eng.*, 1975, **15**, 193–196, translated from Kogaku, 1962, **26**, 1085–1088
6 Tan, C. W., and Hsu, C. J. Low peclet number mass transfer in laminar flow through circular tubes. *Int. J. Heat Mass Transfer*, 1972, **15**, 2187–2201
7 Newman, J. The graetz problem. *The Fundamental Principles of Current Distribution and Mass Transport in Electrochemical Cells* (A. J. Bard, ed.). Dekker, New York, 1973, 198–352
8 Michelsen, M. L., and Villadsen, J. The graetz problem with axial heat conduction. *Int. J. Heat Mass Transfer*, 1974, **7**, 1391–1402
9 Bayazitoglu, Y., and Özisik, M. N. On the solution of graetz type problems with axial conduction. *Int. J. Heat Mass Transfer*, 1980, **23**, 1399–1402
10 Schmidt, F. W., and Zeldin, B. Laminar flows in inlet sections of tubes and ducts. *AICheE J.*, 1969, **15**, 612–614
11 Verhoff, E. H., and Fisher, D. P. A numerical solution of the graetz problem with axial conduction included. *J. Heat Transfer*, 1973, **95**, 132–134
12 Papoutsakis, E. Nusselt numbers near the entrance of heat-exchange section in flow systems. *AIChE J.*, 1981, **27**, 687–689
13 Einstein, T. H. Radiant heat transfer to absorbing gases enclosed in a circular pipe with conduction, gas flow and internal heat generation. NASA TR R-156, 1963
14 Pearce, B. E., and Emery, A. Heat transfer by thermal radiation and laminar forced convection to an absorbing fluid in the entry region of a pipe. *J. Heat Transfer*, 1970, **92**, 221–230
15 Echigo, R., Hasegawa, S., and Kinamuto, K. Composite heat transfer in a pipe with thermal radiation of two-dimensional propagation in connection with the temperature rise in a flowing medium. *Int. J. Heat Mass Transfer*, 1975, **18**, 1149–1159
16 Yener, Y., and Fong, T. M. I. Radiation and forced convection interaction in thermally developing laminar flow through a circular pipe. *Proc. 8th Int. Heat Transfer Conf.*, 1986, **2**, 785–790
17 Campo, A., and Schuler, C. Thermal radiation and laminar forced convection in a gas pipe flow. *Wärme-und Stoffübertragung*, 1988, **22**, 251–257
18 Özisik, M. N. *Radiative Transfer and Interactions with Conduction and Convection.* John Wiley, New York, 1973
19 Kim, T. K., and Lee, H. S. Two-dimensional anisotropic scattering radiation in a thermal developing poiseuille flow. *J. Thermophysics Heat Transfer*, 1990, **2**, 292–298
20 Patankar, S. V. *Numerical Heat Transfer and Fluid Flow.* Hemisphere, Washington, DC, 1980
21 Lii, C. C., and Özisik, M. N. Heat transfer in an absorbing emitting, and scattering slug flow between parallel plates. *J. Heat Transfer*, 1973, **95**(C), 538–540
22 Sparrow, E. M., and Cess, R. D. *Radiation Heat Transfer.* Hemisphere, Washington, DC, 1978